Algorithms for Real-Time Estimation of Individual Wheel Tire-Road Friction Coefficients

Rajesh Rajamani, Gridsada Phanomchoeng, Damrongrit Piyabongkarn, and Jae Y. Lew

***Abstract*—It is well recognized in the automotive research community that knowledge of the real-time tire-road friction coefficient can be extremely valuable for active safety applications, including traction control, yaw stability control and rollover prevention. Previous research results in literature have focused on the estimation of average tire-road friction coefficient for the entire vehicle. This paper explores the development of algorithms for reliable estimation of independent friction coefficients at each individual wheel of the vehicle. Three different observers are developed for the estimation of slip ratios and longitudinal tire forces, based on the types of sensors available. After estimation of slip ratio and tire force, the friction coefficient is identified using a recursive least-squares parameter identification formulation. The observers include one that utilizes engine torque, brake torque, and GPS measurements, one that utilizes torque measurements and an accelerometer and one that utilizes GPS measurements and an accelerometer. The developed algorithms are first evaluated in simulation and then evaluated experimentally on a Volvo XC90 sport utility vehicle. Experimental results demonstrate the feasibility of estimating friction coefficients at the individual wheels reliably and quickly. The sensitivities of the observers to changes in vehicle parameters are evaluated and comparisons of robustness of the observers are provided.**

***Index Terms*—Estimation, observer, tire-road friction coefficient, vehicle dynamics.**

I. Introduction

THE knowledge of tire-road friction coefficient can be extremely useful to many active vehicle safety control systems, including traction control, yaw stability control and rollover prevention control systems. In particular, reliable estimation of the individual friction coefficients at each of the wheels of the vehicle will enable both traction and stability control systems to provide optimum drive torque and/or brake inputs to the individual wheels so as maximize traction, reduce skid, and enhance stability. Many research papers in literature on stability control have also proposed the explicit use of friction coefficient information in calculations of desired yaw rate and other control system variables ([11], [12]). This paper focuses on development and experimental evaluation of algorithms for real-time estimation of tire-road friction coefficients at individual tires of the vehicle.

The tire-road friction coefficient at any tire of the vehicle is defined formally as follows. Let F_x, F_y, and F_z be the longitudinal, lateral, and normal forces acting on a tire. The normalized traction force for the tire, ρ, is defined as

$$\rho := \frac{\sqrt{F_x^2 + F_y^2}}{F_z}. \tag{1}$$

If we consider only longitudinal motion of the vehicle and assume that the lateral force F_y can be neglected for the maneuver under consideration, then

$$\rho := \frac{F_x}{F_z}. \tag{2}$$

The normalized traction force ρ is typically a function of both slip ratio σ_x and the tire-road friction coefficient μ. The tire road-friction coefficient μ on any given road surface is defined as the maximum value that ρ can achieve on that surface for any slip ratio value [9].

II. Review of Previous Results

Several different approaches have been proposed in the literature for the real-time estimation of tire-road friction coefficient. These include the use of an acoustic microphone to listen to the tire ([1], [3]) and the use of optical sensors to investigate road reflections [3].

Researchers have also tried to utilize the measurement of the vehicle motion itself to obtain an estimate of the tire-road friction coefficient. Two types of friction estimation systems have been studied in this area:

1) systems that utilize longitudinal vehicle dynamics and longitudinal motion measurements;
2) systems that utilize lateral vehicle dynamics and lateral motion measurements.

The lateral system can be utilized primarily while the vehicle is being steered. The reader is referred to [6] for a discussion of lateral vehicle motion-based systems.

Longitudinal motion-based systems are in general applicable during vehicle acceleration and deceleration. The most well-known research in this area is on the use of "slip-slope" for friction coefficient identification ([4], [7], [8], [14]). In addition to the slip-slope-based approaches, a Kalman filter-based approach to tire-road friction coefficient identification has been studied in [10]. Researchers have also studied the estimation of friction forces in wheeled robots [16], [17], [18].

Manuscript received September 13, 2010; revised December 11, 2010, February 26, 2011, and April 27, 2011; accepted May 14, 2011. Date of publication July 22, 2011; date of current version August 24, 2012. Recommended by Technical Editor G. Herrmann.

R. Rajamani and G. Phanomchoeng are with the University of Minnesota, Minneapolis, MN 55455 USA (e-mail: rajamani@me.umn.edu, phano002@umn.edu).

D. Piyabongkarn and J. Y. Lew are with the Innovation Center, Eaton Corporation, Eden Prairie, MN 55344 USA (e-mail: NengPiyabongkarn@eaton.com, JaeYLew@eaton.com).

Color versions of one or more of the figures in this paper are available online at http://ieeexplore.ieee.org.

Digital Object Identifier 10.1109/TMECH.2011.2159240

An important point to be noted is that much of the published results in literature focus on estimation of "average" friction coefficient for the vehicle. An exception is the experimental work presented in [19], wherein experimental field data is used for offline estimates of tire forces using an extended Kalman filter and subsequent identification of friction coefficient using Bayesian selection. Different from the work in [19], this paper develops real-time friction coefficient estimation algorithms based on slip-slope calculations for each tire and explores the use of several different sensor systems for friction coefficient estimation.

III. Longitudinal Vehicle Model

The vehicle model utilized consists of equations for the longitudinal motion of the vehicle, for the rotational dynamics of each wheel and for the relationship between tire force, slip ratio, and tire road friction coefficient.

The longitudinal dynamics can be represented as

$$m\dot{V}_x = F_x - R_x - C_a V_x^2 + mg\sin(\theta) \tag{3}$$

where V_x is the longitudinal speed, m is the mass of the vehicle, R_x is the rolling resistance, C_a is an aerodynamic drag parameter, and θ is the road gradient. The total longitudinal tire force is represented by F_x and is the summation of the tire forces generated at all the four tires

$$F_x = F_{xf\ell} + F_{xfr} + F_{xr\ell} + F_{xrr}. \tag{4}$$

Note that the first subscript in the tire force notation refers to the front or rear wheel while the second subscript refers to left or right wheel. In (3), the vehicle is assumed to be undergoing longitudinal motion only and the other degrees of freedom are ignored.

The rotational dynamics of each wheel is represented by

$$I_w\dot{\omega}_i = T_{dr_i} - T_{br_i} - r_{\text{eff}}F_{xi} \tag{5}$$

where the subscript $i = f\ell, fr, r\ell, rr$ is used to separately represent the four wheels of the vehicle. T_{dr_i}, T_{br_i}, r_{eff} , and F_{xi} represent the drive and brake torque delivered to the specific wheel, the effective radius of the tire and the longitudinal tire force of that specific wheel, respectively.

The longitudinal force generated at each tire is known to depend on the longitudinal slip ratio, the tire-road friction coefficient, and the normal force applied at the tire. Longitudinal slip ratio is defined as

$$\sigma_x = \frac{(r_{\text{eff}}\omega_w - V_x)}{V_x} \text{ during braking} \tag{6}$$

$$\sigma_x = \frac{(r_{\text{eff}}\omega_w - V_x)}{(r_{\text{eff}}\omega_w)} \text{ during acceleration.} \tag{7}$$

The tire model utilized to represent the tire force is discussed further in Section IV-B of this paper ([5], [9]).

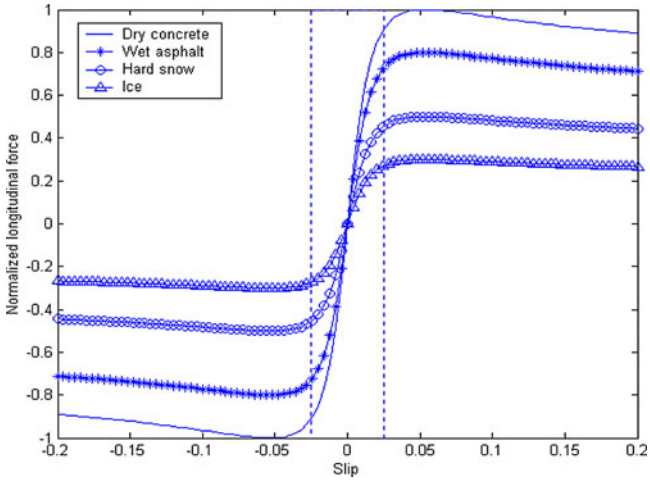

Fig. 1. Longitudinal force versus slip relationship.

IV. Overall Approach to Individual Wheel Tire-Road Friction Estimation

A. Description of Approach

The overall approach used in this paper for individual wheel friction coefficient estimation consists of the following three steps.

1) Estimate the longitudinal tire force at the wheel.
2) Measure or estimate the longitudinal slip ratio at the wheel.
3) Use a recursive least-squares parameter identification algorithm to calculate the tire-road friction coefficient.

Three different algorithms are considered for steps 1 and 2, based on the types of sensors available. Algorithm 1 relies on engine torque measurements and brake torque measurements available over the CAN bus of the vehicle and on inertial vehicle speed measured using a carrier-phase-based GPS system. This is the simplest and most convenient algorithm to utilize. However, a GPS system is an expensive sensor and cannot always be utilized due to satellite drop-outs in urban environments. Algorithm 2 therefore utilizes engine torque and brake torque measurements and a longitudinal accelerometer for the estimation algorithm. Note that engine torque and brake torque signals are typically available over the CAN bus of newer vehicles and do not require any additional sensors for their measurement. Algorithm 3 takes yet another approach of assuming that engine torque measurements are not available and utilizes only a longitudinal accelerometer and GPS-based vehicle speed measurement. All the three algorithms assume that wheel speed measurements are available.

In step 3, the friction coefficient at the tire is calculated based on the values of tire force and slip ratio obtained from steps 1 and 2. Step 3 is discussed further in the next three sections.

B. Tire Model

Fig. 1 shows the traction and braking force versus slip ratio relationship for a variety of road surfaces computed using a tire model. As the figure shows, $\rho = F_x/F_z$ is an increasing function

of slip ratio σ_x until a critical slip value, where ρ reaches a value equal to μ and then starts decreasing slowly.

From the aforementioned figure it is clear that if slip ratio and the normalized tire force are both available, then the tire-road friction coefficient can be calculated, except at very small slip ratios (<0.005).

In the low-slip region (or the linear part of the tire force curves), the longitudinal force generated at an individual tire is proportional to its slip ratio for any given road surface and normal force. This relationship can be described as

$$\rho = \frac{F_x}{F_z} = K\sigma_x \tag{8}$$

where *K* is the slip-slope, whose value changes with road surface conditions and can be directly used to predict the value of the friction coefficient μ. Equation (8) holds for an individual tire.

Equation (8) can be rewritten in a standard parameter identification format as

$$y(t) = \varphi^T(t)\theta(t) \tag{9}$$

where $y(t) = F_x/F_z$ is the system output, $\theta(t) = K$ is the unknown parameter, and $\varphi(t) = \sigma_x$ is the system input. The only unknown parameter *K* can be identified in real time using parameter identification approaches as will be addressed in the next section. Once the slip-slope *K* is identified, it can be used to calculate the tire-road friction coefficient.

Note that the aforementioned slip-slope-based approach is for low slip ratios (linear part of the force-slip curves) only. If the slip ratio is high, as in a hard braking situation, the tire works outside the linear relationship between normalized force and slip ratio and the slip-slope-based method fails in this region. Fortunately, in the high-slip region, the normalized force ρ can be directly used to classify the road surface friction level [13]. The relationship in this case can again be written in standard parameter identification form as $y(t) = \varphi^T(t)\theta(t)$, where $y(t) = F_x$ is the measured longitudinal force, $\theta(t) = \mu$ is the unknown parameter, and $\varphi^T(t) = F_z^T = F_z$ is the normal force.

C. Recursive Least-Squares (RLS) Identification

The slip-slope model described in the previous section can be formulated in a parameter identification form as

$$y(t) = \varphi^T(t)\theta(t) + e(t) \tag{10}$$

where $\theta(t)$ is the vector of estimated parameters, $\varphi(t)$ is the regression vector, $e(t)$ is the identification error between measured $y(t)$ and estimated value $\varphi^T(t)\theta(t)$.

The recursive least-squares algorithm [15] will be used in this paper to iteratively update the unknown parameter vector, $\theta(t)$, at each sampling time, using the past input and output data contained within the regression vector, $\varphi(t)$. The RLS algorithm updates the unknown parameters so as to minimize the sum of the squares of the modeling errors. The procedure of the RLS algorithm at each step *t* is as follows.

Step 1: Measure the system output, $y(t)$, and calculate the regression vector $\varphi(t)$.

Step 2: Calculate the identification error, $e(t)$, which is the difference between system actual output at this sample and the predicted model output obtained from the estimated parameters in previous sample, $\theta(t-1)$, i.e.,

$$e(t) = y(t) - \varphi^T(t)\theta(t-1). \tag{11}$$

Step 3: Calculate the update gain vector, $K(t)$, as

$$K(t) = \frac{P(t-1)\varphi(t)}{\lambda + \varphi^T(t)P(t-1)\varphi(t)} \tag{12}$$

and calculate the covariance matrix, $P(t)$, using

$$P(t) = \frac{1}{\lambda}\left[P(t-1) - \frac{P(t-1)\varphi(t)\varphi^T(t)P(t-1)}{\lambda + \varphi^T(t)P(t-1)\varphi(t)}\right]. \tag{13}$$

Step 4: Update the parameter estimate vector, $\theta(t)$, as

$$\theta(t) = \theta(t-1) + K(t)e(t). \tag{14}$$

The parameter, λ, in the aforementioned equations, is called the forgetting factor. It is used to effectively reduce the influence of old data which may no longer be relevant to the model, and therefore prevent a covariance wind-up problem. This allows the parameter estimates to track changes in the process quickly. A typical value for λ is in the interval (0.9, 1).

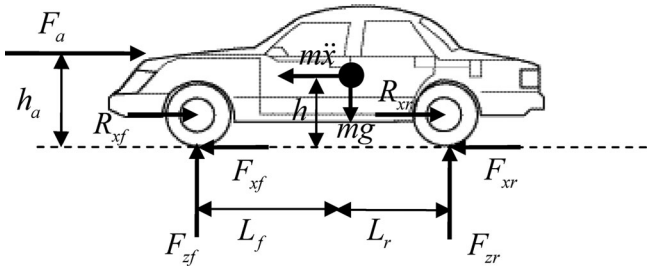

Fig. 2. Vehicle longitudinal dynamics schematic.

D. Determination of the Normal Force

As seen from the friction coefficient estimation (8), the normal force plays an important role in determining the maximum force the tire can generate. For the same road surface and tire, the larger the normal force, the larger the longitudinal force could be. The mass of the vehicle contributes a major portion of the normal force, and the other forces acting on the vehicle during longitudinal maneuvers redistribute the normal forces between the tires [9].

If the vehicle is traveling in a straight line on level road, the normal forces at the front and rear tires can be calculated using a static force model of the vehicle as shown in Fig. 2 [13]

$$F_{zf} = \frac{mgL_r - ma_x h - C_a V_x^2 h_a}{L} \tag{15}$$

$$F_{zr} = \frac{mgL_f + ma_x h + C_a V_x^2 h_a}{L} \tag{16}$$

$F_{zfl} = F_{zfr} = \frac{F_{zf}}{2}$, $F_{zrl} = F_{zrr} = \frac{F_{zr}}{2}$, the vehicle mass *m*, wheelbase $L = L_f + L_r$, and lengths L_f and L_r are measured and assumed to be constant.

E. Calculation of Friction Coefficient

The estimated slip-slope varies with the road surface and is used to calculate tire-road friction coefficient. Based on experimental data described later in the paper, the following linear equation is found to express the observed relationship between slip-slope and friction coefficient:

$$\mu = AK + C \tag{17}$$

where K is the slip-slope, $A = 0.026$ is the proportionality constant and $C = 0.047$ is a bias constant.

V. Friction Estimation using GPS and Torque Measurements

For each wheel, the rotational dynamics is given by

$$I_w \dot{\omega} = T_{dr} - T_{br} - r_{\text{eff}} F_x \tag{18}$$

where the subscripts have been omitted for convenience. The same estimator and equations hold for all wheels. The following estimator which avoids the need to take derivatives of ω is proposed for estimating the longitudinal force F_x

$$I_w \dot{\hat{\omega}} = T_{dr} - T_{br} - r_{\text{eff}} \hat{F}_x + \ell \tilde{\omega} \tag{19}$$

$$\dot{\hat{F}}_x = -\eta \tilde{\omega} \tag{20}$$

where $\tilde{\omega} = \omega - \hat{\omega}$ is the estimation error for wheel speed, $\tilde{F}_x = F_x - \hat{F}_x$ is the estimation error for tire force, and η is a positive gain. The effective tire radius r_{eff} is assumed to be known. Subtracting (19) from (18), the estimation error dynamics are seen to be given by

$$I_w \dot{\tilde{\omega}} = -r_{\text{eff}} \tilde{F}_x - \ell \tilde{\omega} \tag{21}$$

or, after differentiation,

$$\Rightarrow I_w \ddot{\tilde{\omega}} + \ell \dot{\tilde{\omega}} + r_{\text{eff}} \eta \tilde{\omega} = 0. \tag{22}$$

Thus, with the observer gain ℓ being positive, we have $\tilde{\omega} \to 0$, $\dot{\tilde{\omega}} \to 0$. Since the estimation error dynamics are given by (21), it follows that $\tilde{F}_x \to 0$ as $t \to \infty$.

The proposed observer of (19) and (20) thus ensures stable estimation of the longitudinal tire force.

The slip ratio can be directly calculated using (6) and (7) in this algorithm, since vehicle speed is available from GPS and wheel speeds are also measured.

As described in Section IV, once the longitudinal tire force and slip ratio have been estimated, the tire road coefficient can be estimated using a recursive least-squares parameter identification technique.

A. Simulation Results

The proposed longitudinal force estimation algorithm is evaluated in simulations by implementing it in CARSIM, an industry-standard vehicle dynamics simulation software. The vehicle model from CARSIM chosen for this simulation is a D-Class sedan with default parameters ($m = 1530$ kg, $I_w = 1\,\text{kg.m}^2$, $r_{\text{eff}} = 0.335$ m). The D-Class sedan is a front-wheel drive vehicle. The force distribution ratio between the front left and front right wheel is 0.5. The tire model is based on the

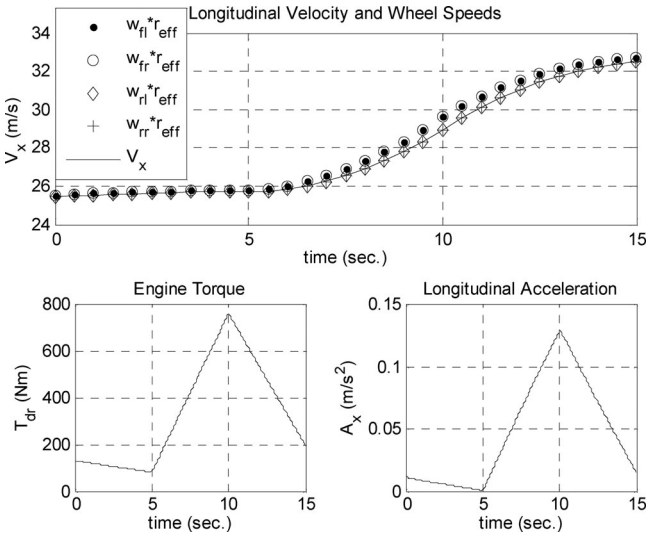

Fig. 3. Longitudinal speed, wheel speeds, engine torque, and longitudinal acceleration.

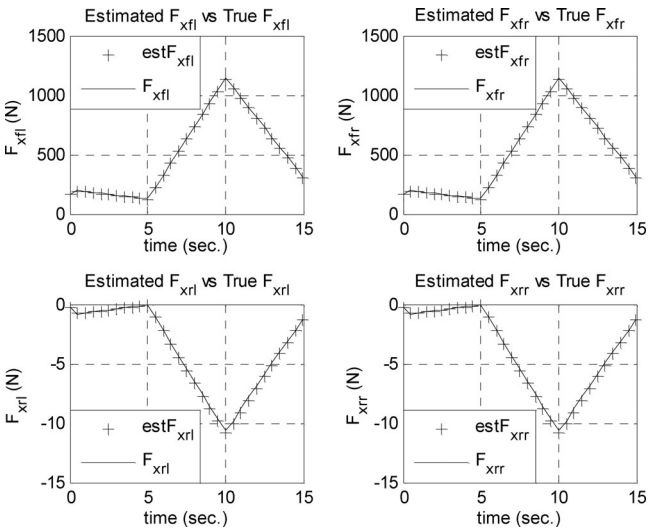

Fig. 4. Estimated longitudinal forces versus true longitudinal forces.

Pacejka magic formula model [9]. It should be noted that while the longitudinal force estimation algorithm was developed using the simple model of (18), the simulations are being conducted using a high-fidelity commercial vehicle dynamics model. At the beginning of the simulation, the speed of the vehicle is kept constant at about 25.5 m/s. After that, the vehicle starts accelerating. The vehicle is accelerated to 33.5 m/s. The first row of Fig. 3 shows the longitudinal speed and wheel speeds of this simulation. The engine torque and longitudinal acceleration are presented in the second row of Fig. 3.

The comparison of the estimated longitudinal forces using the algorithm described in this section and simulated forces using the CarSim software is presented in Fig. 4. The results show that the estimated longitudinal forces closely match the simulated forces. Also, those estimated forces converge very quickly to the simulated forces. Fig. 3 also shows the relationship between

the forces and engine torque. The shapes of the force curves are similar to the shape of the engine torque curve.

An experimental evaluation of this longitudinal force estimation and tire-road friction coefficient estimation algorithm is presented in Section VIII of this paper.

VI. Friction Estimation Using Torque Measurements and an Accelerometer

A. Using Torque Measurements and one Accelerometer

In this case the observer for estimation of longitudinal tire force remains the same as in Section V. However, an estimator is needed for the estimation of longitudinal vehicle speed, since GPS measurements are no longer available. The longitudinal dynamics of the vehicle are

$$m\dot{V}_x = F_x - R_x - C_a V_x^2 + mg\sin(\theta). \tag{23}$$

Note that the road gradient in (23) is also unknown and must be estimated. The proposed observer for vehicle speed can be written as

$$m\dot{\hat{V}}_x = F_x - R_x - C_a \hat{V}_x^2 - me \tag{24}$$

$$\dot{e} = -\frac{1}{\tau}e + \frac{1}{\tau}a_{\text{meas}} - \frac{1}{\tau}\dot{\hat{V}}_x \tag{25}$$

where the longitudinal accelerometer measures both acceleration and a component of gravity due to road gradient and its measurement is given by

$$a_{\text{meas}} = \dot{V}_x - g\sin(\theta). \tag{26}$$

Let $\tilde{V}_x = V_x - \hat{V}_x$ be the estimation error. The constant τ is a positive gain.

Claim: The observer given by (24) and (25) provides asymptotically stable estimates of both longitudinal vehicle speed and the road-gradient angle θ.

Proof: First, by subtracting (24) from (23), we find

$$\dot{\tilde{V}}_x = -C_a\left(V_x^2 - \hat{V}_x^2\right)/m + [g\sin(\theta) + e]. \tag{27}$$

Dynamics of e:

$$\begin{aligned}\dot{e} &= -\frac{1}{\tau}e + \frac{1}{\tau}a_{\text{meas}} - \frac{1}{\tau}\dot{\hat{V}}_x \\ &= -\frac{1}{\tau}e + \frac{1}{\tau}\left[-\frac{C_a}{m}(V_x^2 - \hat{V}_x^2) + g\sin(\theta) + e\right] - \frac{1}{\tau}g\sin(\theta) \\ &= -\frac{C_a}{\tau m}(V_x^2 - \hat{V}_x^2).\end{aligned} \tag{28}$$

Dynamics of $\tilde{V}_x$:

Substituting (28) into (27)

$$m\dot{\tilde{V}}_x = -C_a(V_x^2 - \hat{V}_x^2) + mg\sin(\theta) - \int \frac{C_a}{\tau}(V_x^2 - \hat{V}_x^2)dt. \tag{29}$$

Note that $(V_x^2 - \hat{V}_x^2)$ can be written as $(V_x + \hat{V}_x)(V_x - \hat{V}_x)$ and that $(V_x + \hat{V}_x)$ is always positive. Equation (29) is therefore the same as the error dynamics of a PI controller with a constant disturbance input $mg\sin(\theta)$. Hence, $\tilde{V}_x \to 0$ as $t \to \infty$. Also $e \to -g\sin(\theta)$ as $t \to \infty$.

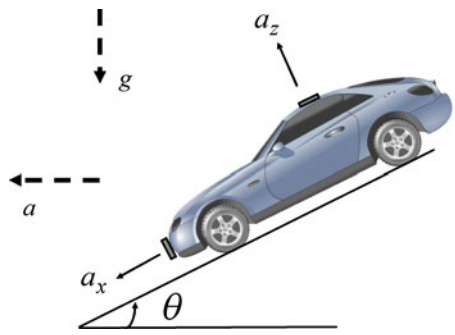

Fig. 5. Two accelerometer analysis.

The aforementioned observer is stable and leads to stable estimates of road gradient and vehicle speed. However, a disadvantage of the proposed observer is that the damping in the closed-loop estimation error dynamics is determined entirely by the aerodynamic drag parameter C_a. This damping is typically low and leads to under-damped estimation dynamics.

B. Using Torque Measurements and Two Accelerometers

The observer in Section VI-A can estimate both vehicle speed and road gradient but yields underdamped estimation error dynamics. This section proposes an alternate observer that utilizes two accelerometers—a longitudinal accelerometer and a vertical accelerometer to estimate road gradient and vehicle speed.

First, the road gradient is estimated by analyzing the components of accelerations measured by the two accelerometers. Consider the system shown in Fig. 5. The accelerometer readings are denoted by a_x and a_z, while the two orthogonal components of acceleration acting on the vehicle are assumed to be a and g, respectively. g is the acceleration due to gravity and is known to be 9.81 m/s^2.

The readings of the two accelerometers are

$$a_x = a\cos(\theta) - g\sin(\theta) \tag{30}$$

$$a_z = a\sin(\theta) + g\cos(\theta). \tag{31}$$

Solving (30) and (31) simultaneously,

$$a = \sqrt{a_x^2 + a_z^2 - g^2} \tag{32}$$

$$\sin(\theta) = \frac{aa_z - ga_x}{a^2 + g^2} \tag{33}$$

$$\cos(\theta) = \frac{a_z g + aa_x}{a^2 + g^2}. \tag{34}$$

The sign of a must be chosen such that (33) and (34) yield consistent values of θ.

After the road gradient has been estimated using (33)–(34), the longitudinal vehicle speed is estimated using a combination of longitudinal accelerometer and wheel speed sensors. The observer for this purpose is as follows.

Define the bias error in the accelerometer after correcting for road gradient as

$$\varepsilon(k) = a_{\text{meas}}(k) + g\sin(\theta) - a_{\text{real}}(k). \tag{35}$$

The longitudinal velocity of the vehicle can be represented as

$$V_x(k) = V_x(k-1) + \Delta T \cdot a_{\text{meas}}(k) + g\sin(\theta) + w(k) \tag{36}$$

and the rotational wheel speed can be represented as

$$\omega(k) = 1/R_{\text{eff}} \cdot V_x(k) + n(k) \tag{37}$$

where $w(k)$ and $n(k)$ are sensor noise. The rotational speed $\omega(k)$ is chosen from an appropriate wheel or a combination of wheel speeds. The longitudinal velocity can be obtained by the following discrete time Kalman filter:

$$\hat{V}_x(k) = \hat{V}_x(k-1) + \Delta T \cdot a_{\text{meas}}(k) + K\left(\omega(k) - \frac{1}{R_{\text{eff}}}(\hat{V}_x(k-1) + \Delta T \cdot a_{\text{meas}}(k)\right) \tag{38}$$

where the constant K is a positive gain whose value is chosen so as to address the trade-off between accelerometer integration drift and noise in the wheel speed sensor. Note that in this observer the bias in the accelerometer readings is corrected by the use of feedback of wheel speed. The experimental performance of this observer for estimation of road gradient is discussed in Section VIII.

VII. Friction Estimation Using GPS and an Accelerometer

Since the longitudinal speed and wheel speeds are known, the longitudinal slip ratio can be calculated using (6) and (7). In the absence of engine and/or brake torque measurements, the following equations involving longitudinal vehicle dynamics and wheel rotational dynamics can be utilized to estimate the variables of drive torque, individual longitudinal tire forces and road gradient

$$m\dot{V}_x = (F_{xf\ell} + F_{xfr} + F_{xr\ell} + F_{xrr}) - R_x - C_a V_x^2 + mg\sin(\theta) \tag{39}$$

$$I_w\dot{\omega}_{f\ell} = aT_q - r_{\text{eff}}F_{xf\ell} \tag{40}$$

$$I_w\dot{\omega}_{fr} = bT_q - r_{\text{eff}}F_{xfr} \tag{41}$$

$$I_w\dot{\omega}_{r\ell} = cT_q - r_{\text{eff}}F_{xr\ell} \tag{42}$$

$$I_w\dot{\omega}_{rr} = dT_q - r_{\text{eff}}F_{xrr} \tag{43}$$

where T_q is total torque and can be due to engine or brake. a, b, c, and d are force distribution ratios used to determine the fraction of total torque, T_q, applied to each wheel. (Note: $a+b+c+d=1$.) For example, $a=0.5$, $b=0.5$, and $c=d=0$ for total torque of a front wheel drive vehicle.

Since the absolute vehicle speed V_x is measured using GPS and the corrected acceleration of the vehicle $\dot{V}_x - g\sin\theta$ is measured using a longitudinal accelerometer, there are five unknowns in the five (39)–(43). This can be solved to obtain $F_{xf\ell}$, F_{xfr}, $F_{xr\ell}$, and $F_{xrr}$and T_q. Road gradient can be calculated subsequently. A stable observer as described earlier in Section V can also be designed for this purpose so as to avoid differentiation. The following estimator which avoids the need to take derivatives of ω is proposed for estimating the longitudinal force F_x and total torque T_q:

$$\begin{bmatrix}\dot{\hat{V}}_x\\ \dot{\hat{\omega}}_i\\ \dot{\hat{F}}_{xi}\\ \dot{\hat{T}}_q\end{bmatrix} = \begin{bmatrix}0&0&p&0\\0&0&r&q\\0&0&0&0\\0&0&0&0\end{bmatrix}\begin{bmatrix}\hat{V}_x\\ \hat{\omega}_i\\ \hat{F}_{xi}\\ \hat{T}_q\end{bmatrix} + \begin{bmatrix}-1&-1\\0&0\\0&0\\0&0\end{bmatrix}\begin{bmatrix}\frac{C_aV_x^2}{m}\\ \frac{R_x}{m}\end{bmatrix} + K_a\left(\begin{bmatrix}\sum F\\ V_x\\ \omega_i\end{bmatrix} - \begin{bmatrix}0&0&s&0\\1&0&0&0\\0&1&0&0\end{bmatrix}\begin{bmatrix}\hat{V}_x\\ \hat{\omega}_i\\ \hat{F}_{xi}\\ \hat{T}_q\end{bmatrix}\right) \tag{44}$$

$$\sum F = m\dot{V}_x + R_x + C_aV_x^2 - mg\sin\theta \tag{45}$$

where $\omega_i = \begin{bmatrix}\omega_{f\ell}\ \omega_{fr}\ \omega_{r\ell}\ \omega_{rr}\end{bmatrix}^T$ $\hat{\omega}_i = \begin{bmatrix}\hat{\omega}_{f\ell}\ \hat{\omega}_{fr}\ \hat{\omega}_{r\ell}\ \hat{\omega}_{rr}\end{bmatrix}^T$, $\hat{F}_i = \begin{bmatrix}\hat{F}_{f\ell}\ \hat{F}_{fr}\ \hat{F}_{r\ell}\ \hat{F}_{rr}\end{bmatrix}^{\text{T}}$, $p = (1/m)[1\ 1\ 1\ 1]$, $q = (1/I_w) \times \begin{bmatrix}a\ b\ c\ d\end{bmatrix}^T$, $r = -(r_{\text{eff}}/I_w)I_{4\times4}$, and $s = \begin{bmatrix}1\ 1\ 1\ 1\end{bmatrix}$. K_a is an observer gain matrix chosen so as to stabilize the error dynamics obtained by the difference between the state equations in (39)–(43) and the estimator dynamics in (44) and (45). The value of K_a is chosen based on desired locations of the closed-loop eigenvalues for this linear time invariant system. The effective tire radius r_{eff} is assumed to be known.

A. Simulation Results

Again, the performance of the observer will be evaluated by simulating the algorithm together with the CarSim software. We use the same CARSIM vehicle model as described in Section V-A. However, in this section, only wheel speeds and acceleration will be used to estimate the longitudinal tire forces.

The comparison of the estimated longitudinal forces using the algorithm described in Section VII and actual forces using the CarSim software is presented in Fig. 7. The results show that the estimated longitudinal forces match the simulated forces very well. Also, those forces converge very quickly to the simulated forces. However, there are some minor errors in the rear wheel longitudinal forces. This may be due to model mismatch with CARSIM.

The first row and second row of Fig. 6 show the estimated engine torque and the longitudinal acceleration, respectively. Again, the minor errors in estimated engine torque may be due to small model errors.

After the longitudinal tire force and slip ratio have been estimated, then the tire road coefficient can be estimated using the algorithm in Section IV-C.

VIII. Experimental Results

This section presents experimental evaluation of the estimation algorithms. In particular, evaluation of the gradient estimation algorithm discussed in Section VI-B, evaluation of the longitudinal tire force estimation algorithms discussed in Sections V, and VII and evaluation of the tire-road friction estimation algorithm discussed in Section IV are presented.

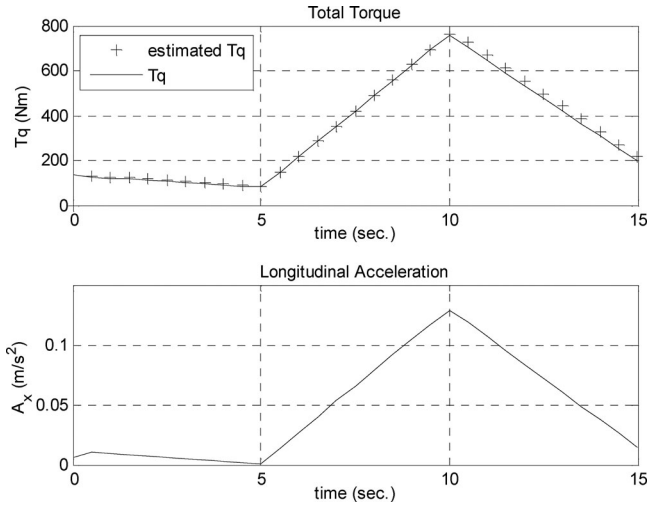

Fig. 6. Estimated engine torque and longitudinal acceleration.

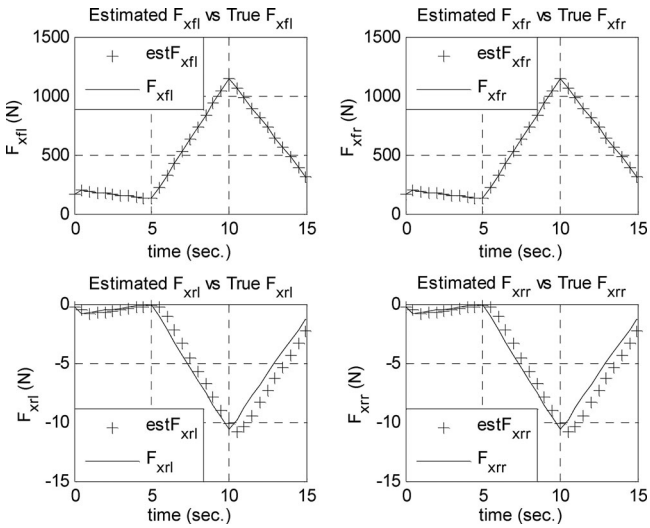

Fig. 7. Estimated longitudinal forces versus true longitudinal forces.

A. Test Vehicle and Experimental Set-Up

The test vehicle used for the experimental evaluation is a Volvo XC90 sport utility vehicle. Vehicle testing was conducted at the Eaton Proving Ground, Marshall, MI. A MicroAutoBox from dSPACE is used for real-time data acquisition. A real-time GPS system, RT3000, from Oxford Technical Solutions is used to obtain absolute vehicle speed, slip angle, and several other variables. The RT3000 is a full, six-axis inertial navigation system with integrated GPS and a Kalman filter that provides high frequency updates of the sensor bias, heading, and vehicle velocities. The GPS outputs were connected to the MicroAutoBox via CAN communication at the baud rate of 0.5 Mbits/s. Engine torque, transmission gear ratio, wheel speeds and several other variables are obtained from the CAN bus signals already available on the CAN network of the Volvo XC90. The sampling time is set at 2 ms. A photograph of the test vehicle is shown in Fig. 8. Key vehicle parameters used in the estimation algorithms are $m = 2205$ kg, $C_a = 0.3693$ $I_w = 0.8$, and $r_{\text{eff}} = 0.3543$.

Fig. 8. Volvo XC90 test vehicle with GPS system.

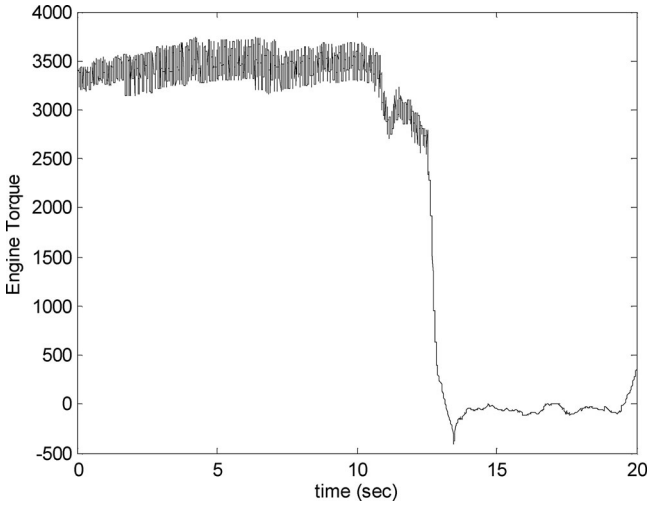

Fig. 9. Engine torque during driving on 60% grade.

B. Road-Gradient Estimation

The road-gradient estimation algorithm was evaluated on several different roads of known gradient. A sample result is presented in this section for driving on a road with a known steep gradient of 60%.

Fig. 9 shows the engine torque input for the maneuver. The maneuver consisted of driving up the steep gradient with a net positive acceleration (increasing speed) and then reducing the throttle and engine torque after reaching the top of the gradient road. In other words, the vehicle decelerated after reaching the top of the road when it moved on a gentler downhill road. Figs. 10 and 11 show the longitudinal and vertical accelerometer readings. The significant acceleration read by the longitudinal accelerometer and the significant deviation of the vertical accelerometer from 9.81 m/s^2 are both due to the significant steep grade of the road. The vehicle reaches the top of the 60% gradient road at about 10 s after which it moves downhill. The road gradient as estimated by the algorithm of Section VI-B is shown in Fig. 12. As seen in the figure, the gradient is estimated correctly and compares well with the actual known grade of the road for the first 10 s of the experiment. Note that a 60% grade is equivalent to a gradient angle of approximately -31°. The transition in road grade from -31 to $+5$ degrees does not occur instantaneously, but occurs gradually in the real road. Since only the initial and final road-grade values are actually known, they have been indicated with dotted lines in Fig. 12. The big change

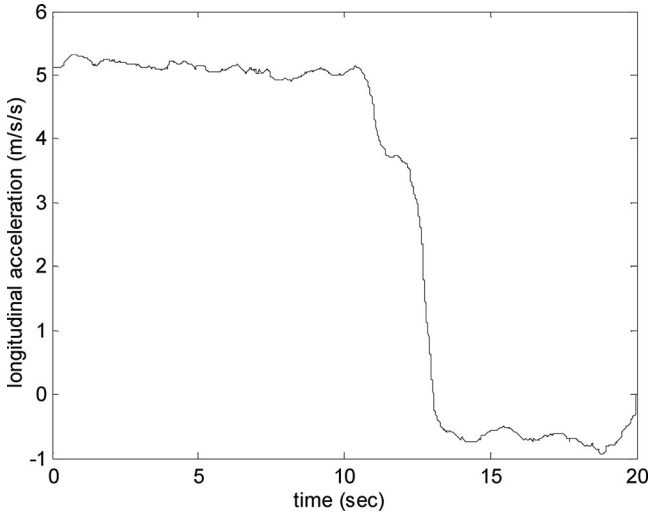

Fig. 10. Longitudinal accelerometer on 60% grade.

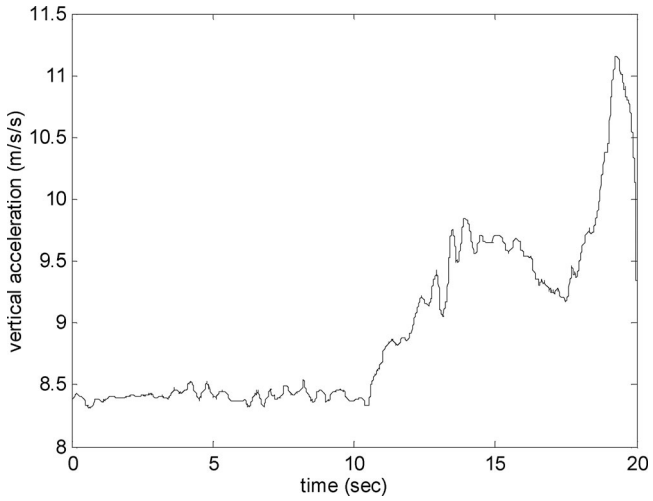

Fig. 11. Vertical accelerometer signal on 60% grade.

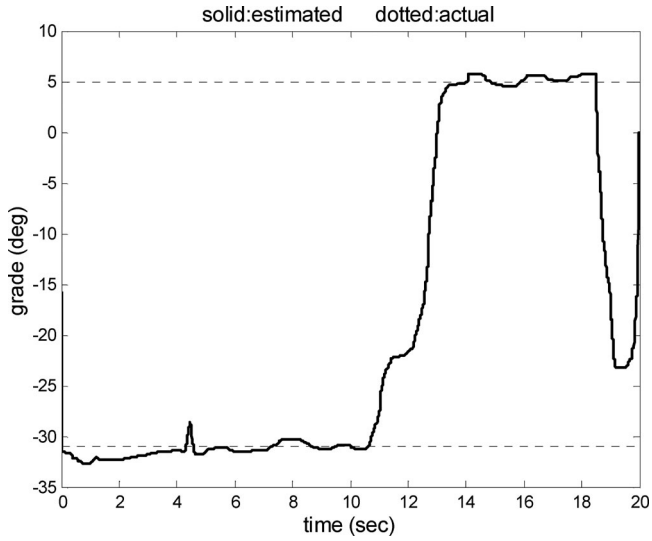

Fig. 12. Estimated gradient of the road.

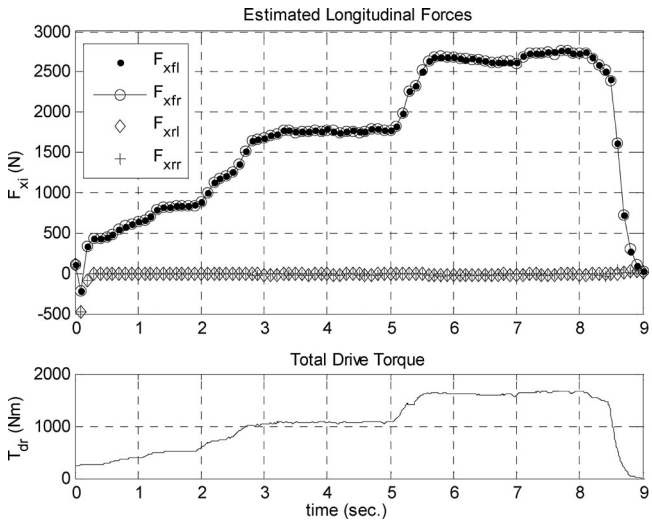

Fig. 13. Drive torque, and estimated longitudinal forces.

in estimate that occurs toward the end around 18 s is because the vehicle briefly stops moving after deceleration.

C. Friction Estimation Using GPS and Torque Measurements

The longitudinal tire forces are estimated by the algorithm described in Section V. In this test, the vehicle moves from a dry asphalt road to a dirt/gravel road surface. Consequently, a drop in friction coefficient occurs during the test. The drive torque which determines vehicle behavior during the test is shown in Fig. 13(b).

The estimated longitudinal tire forces for each wheel are shown in Fig. 13(a). Even though we do not know the true value of longitudinal tire forces, the estimated forces seem reasonable. The estimated forces of the front wheels agree roughly with the engine torque and longitudinal acceleration. Also, the estimated forces of the rear wheels are approximately zero as seen, because the vehicle used front wheel drive mode during the experiment.

Fig. 14 shows longitudinal speed, wheel speeds and acceleration. The change in friction coefficient occurred between 6.5 and 7 s. At this point there is a jump in the front wheel speeds as seen in Fig. 14.

Next, we present the friction estimation experimental results. The friction coefficient is estimated using the algorithm as described in Section IV-B. The system input is slip ratio computed by (6) or (7). The output is F_x/F_z. The normal force, F_z is computed by (15) and (16). The longitudinal tire force is computed by the algorithms in Section V.

The results of the friction estimation algorithm are shown in Fig. 15. The first row of the figure presents the slip ratio versus normalized force of the front-left and front right wheels. We do not show the slip ratio versus normalized force of rear-left wheel and rear-right wheel, since the vehicle is a front-wheel drive vehicle. The longitudinal forces of rear wheels are approximately 0. The estimated slip slopes of front-left wheel and front-right wheel are presented in the second row of the figure. The figure shows that the estimated slip slopes of the front-left and front-right wheels converge from an initial guess

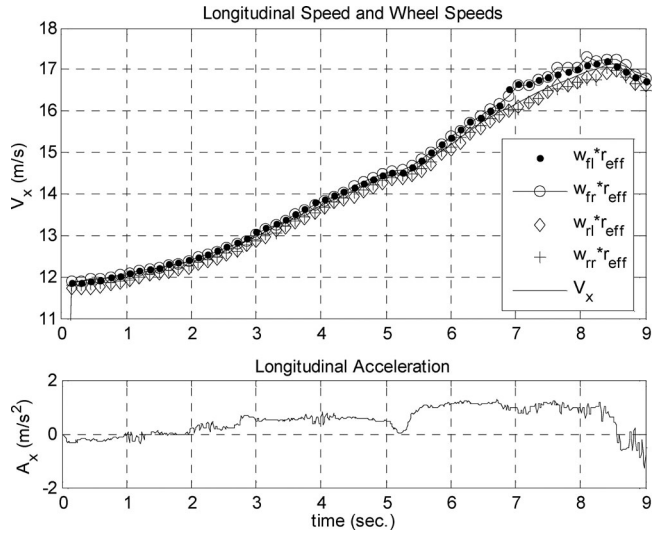

Fig. 14. Longitudinal speed and acceleration and wheel speeds.

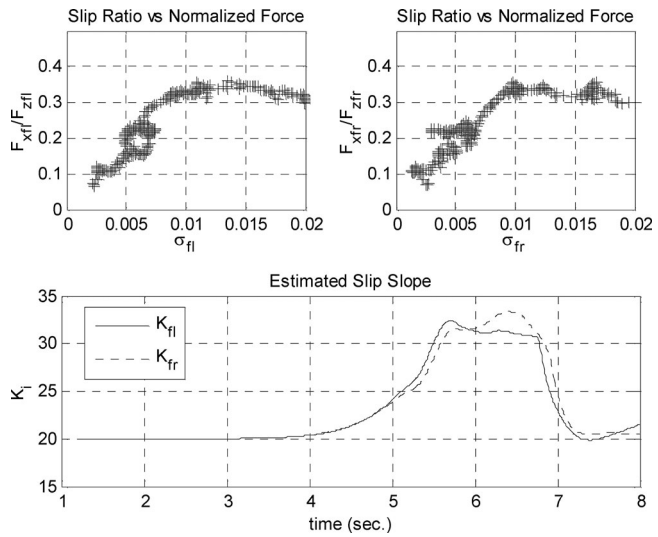

Fig. 15. Step change in the friction coefficient experiment with acceleration during the transition.

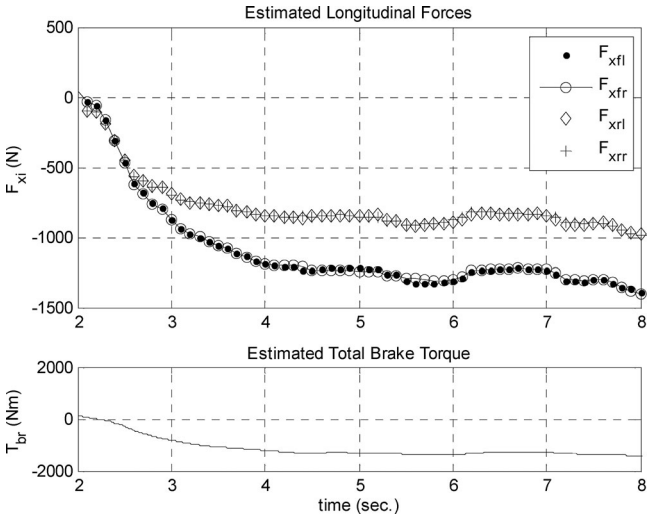

Fig. 16. Estimated brake torque and estimated longitudinal forces.

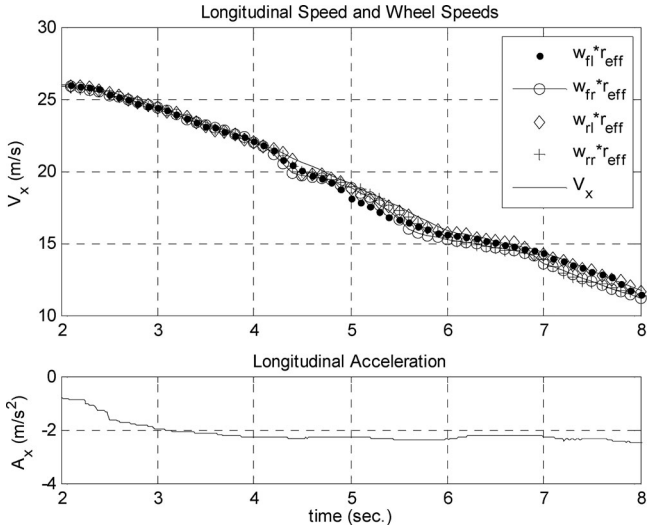

Fig. 17. Longitudinal speed and acceleration and wheel speeds.

value to the estimated slip slope value of about 32 for the first road surface and then converge to another estimated slip slope value of about 21 for the second road surface.

Using a linear relationship between the slip-slope and friction coefficient as described in Section IV-E, the friction coefficient for the dry asphalt road is estimated to be 0.89 and for the gravel surface is estimated to be 0.56. It should be noted that the friction coefficient on dirt/gravel was found to vary between 0.5–0.7. However, the average value is distinctly different from that on dry asphalt and concrete.

D. Estimation Using GPS and an Accelerometer

In this section, the longitudinal tire forces are estimated by using wheel speeds, vehicle speed, and acceleration as described in Section VII. In this test, the vehicle moved from a dry asphalt road surface to an icy surface. The vehicle decelerated due to braking during the road surface transition from asphalt to ice. The brake torque at the individual wheels were not measured and not available over the CAN bus of the vehicle. Hence, the friction coefficient was estimated exclusively using GPS, accelerometer and wheel speed signals.

The estimated longitudinal tire forces for each wheel and the estimated total brake torque are shown in Fig. 16. The shape of the estimation force curves roughly tracks the shape of the acceleration curves. Also, if we compute total longitudinal tire force, the value of total forces is roughly close to the value of mass multiplied by acceleration after subtraction of drag force and rolling resistance force. The estimated forces therefore seem reasonable. Fig. 16 also shows that the longitudinal forces of the front wheels are larger than those of the rear wheels since the braking force distribution ratio between front and rear axles is 60:40.

Fig. 17 shows longitudinal speed, wheel speeds and acceleration. The change in friction coefficient occurred at about

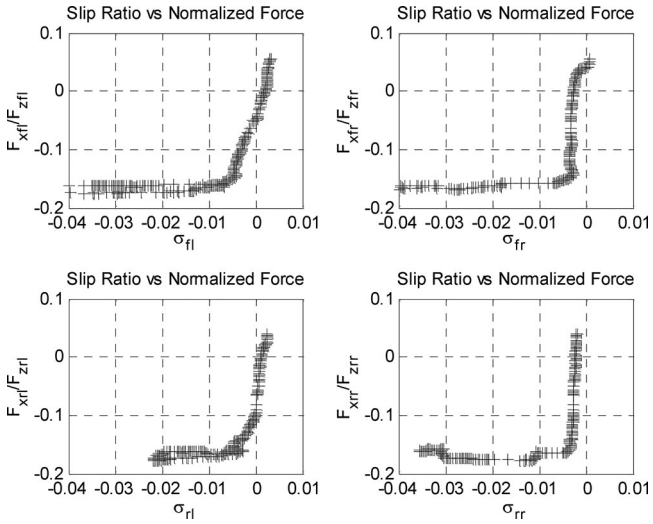

Fig. 18. Step change in the friction coefficient experiment with deceleration during the transition.

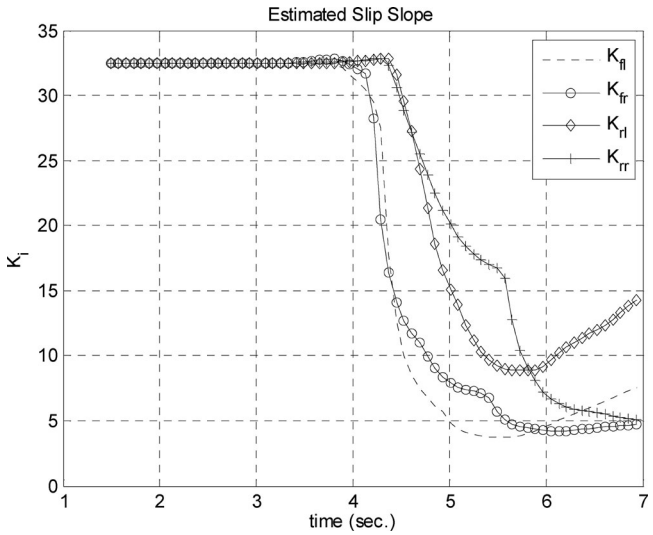

Fig. 19. Step change in the friction coefficient experiment with deceleration during the transition.

4.5 s. At this point a dip in the front wheel speeds can be noticed.

Next, the friction estimation experimental results will be evaluated by using the algorithm as described in Section IV-B. Fig. 18 presents the slip ratio versus normalized force for each wheel. The estimated slip slopes are presented in Fig. 19. Fig. 19 shows that the estimated slip slope of each wheel converges from the slip slope value of about 32.5 for the first road surface to the estimated slip slope value of about 5 for the second road surface. The estimated slip slopes of front wheels start to converge before the estimated slip slopes of the rear wheels. Thus, the slip slopes can be reliably used to classify the friction coefficients of these two road surfaces.

Using the linear relationship between the slip-slope and friction coefficient described in Section IV-E, the friction coefficient for the dry asphalt surface is seen to be approximately 0.89 and for ice to be 0.18.

E. Comparison of the Developed Friction Coefficient Estimation Algorithms

With the relation in (17), the friction coefficient for dry asphalt ($K = 32.5$) is seen to be 0.89. The friction coefficient for dirt/gravel (see Fig. 15, $K = 20$) is seen to be 0.56 and for ice (see Fig. 19, $K = 5$) is seen to be 0.18.

The three friction coefficient estimation methods discussed in this paper have different domains of applicability based on the set of sensors available for the estimation algorithm. However, Algorithm 2 (that utilizes torque measurements and an accelerometer) depends exclusively on aerodynamic drag to provide transient convergence. It is found to be unsuitable, since the aerodynamic drag coefficient is often not large enough to provide good transient performance. Between Algorithms 1 and 3, Algorithm 1 depends only on a wheel-level dynamic model. It involves a simpler computational algorithm and is found to be more accurate and to converge faster than Algorithm 3 which involves a vehicle-level fifth order dynamic model. For example, a comparison of the results in Fig. 4 versus Fig. 7 show that Algorithm 1 provides more accurate estimates of the longitudinal tire forces. However, wheel torque signal measurement may not be available in all applications, while GPS and accelerometer measurements could potentially be provided on all vehicles.

IX. Sensitivity Analysis to Mass Change

A. Friction Estimation Algorithm Using GPS and Torque Measurements

Equations (15) and (16) are used to compute normal forces, F_{zi}. The longitudinal tire forces, F_{xi}, are computed by using the rotational dynamic equations. Subsequently, the normalized traction forces, ρ, are computed

$$\rho = \frac{F_x}{F_z} \tag{46}$$

The slip ratio depends on effective radius, longitudinal speed, and wheel speeds. The slip ratio is not sensitive to mass change. Hence, the only equations that include vehicle mass in the estimation algorithm are (15) and (16)

$$F_{zf} = \frac{mgL_r - ma_x h - C_a V_x^2 h_a}{L}$$

and

$$F_{zr} = \frac{mgL_f + ma_x h + C_a V_x^2 h_a}{L}.$$

To evaluate sensitivity to change in vehicle mass for this algorithm, the sensitivity of the normalized traction forces is first examined, followed by observing the sensitivity of estimated slip slope to mass change. The scenario simulated in Figs. 20–22 consists of vehicle acceleration on dry asphalt and transition of the road surface from dry asphalt to dirt/gravel (a friction coefficient of 0.56). The scenario is similar to the experimental test of Fig. 15.

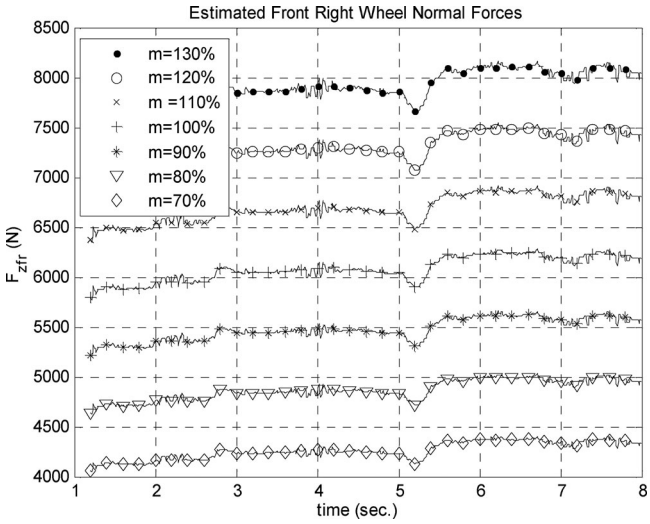

Fig. 20. Estimate front right wheel normal forces.

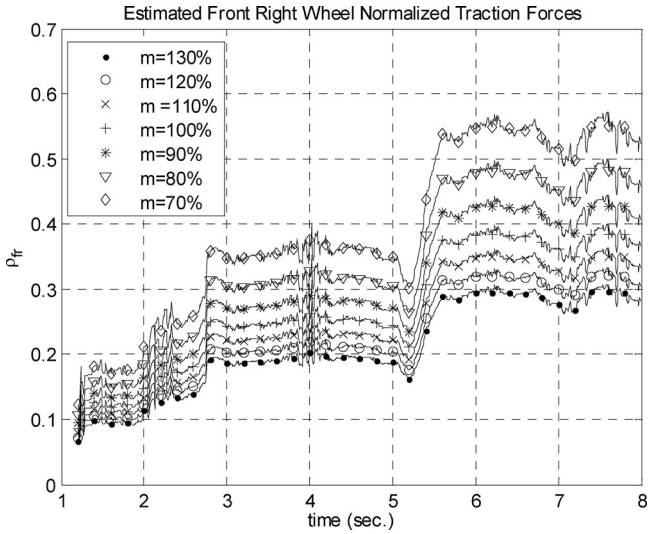

Fig. 21. Estimated front right wheel normalized traction forces.

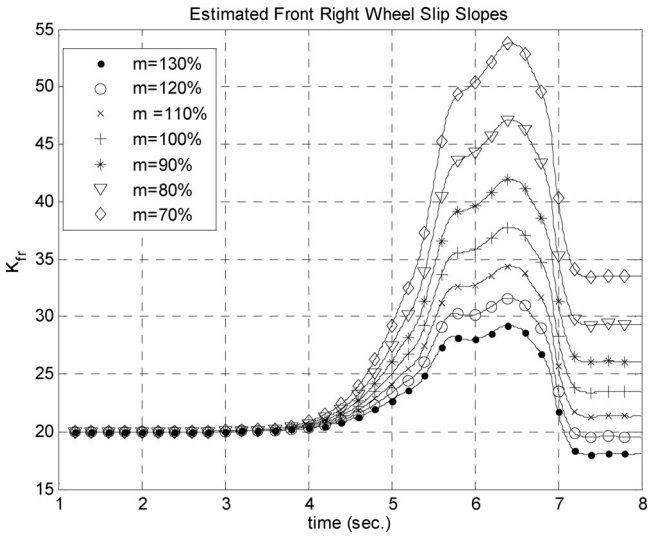

Fig. 22. Estimated front right wheel slip slopes.

Fig. 20 shows the effect of mass change on normal forces. If a_x and C_a are small, the normal force is roughly proportional to mass. The normal force increases when mass increases.

Fig. 21 shows the effect of mass change on normalized traction forces. The normalized traction force is proportional to longitudinal tire force and inversely proportional to normal force. Since mass change affects only the normal force estimate in this algorithm, the normalized traction force changes when the normal force changes.

Fig. 22 shows the effect of mass change on estimated slip slopes. The slip slope changes because the normalized traction forces change while the slip ratio values do not change. Thus this algorithm is seen to be very sensitive to mass change.

To improve the robustness of this algorithm, the value of vehicle mass could be updated in real-time. When the vehicle is first switched on, the vehicle mass can be estimated from Fig. 22, assuming the road pavement is dry concrete and its friction coefficient is known. Subsequently, once the vehicle mass value has been updated, the algorithm will provide correct estimates of friction coefficient as the pavement surface changes.

B. Friction Estimation Algorithm Using GPS and an Accelerometer

The equations that include vehicle mass in the computation are

$$m\dot{V}_x = (F_{xf\ell} + F_{xfr} + F_{xr\ell} + F_{xrr}) - R_x - C_a V_x^2 + mg\sin(\theta) \quad (47)$$

and (15) and (16)

$$F_{zf} = \frac{mgL_r - ma_x h - C_a V_x^2 h_a}{L}$$

and

$$F_{zr} = \frac{mgL_f + ma_x h + C_a V_x^2 h_a}{L}.$$

Equation (47) and the rotational dynamic equations are used to compute longitudinal tire forces. The normal forces, F_{zi}, are computed from (15) and (16). Then the normalized traction forces, ρ, are computed. (The slip ratio does not depend on mass.)

To evaluate sensitivity of the estimation algorithm to mass change, first the sensitivity of the normalized traction forces is examined, followed by examining the sensitivity of the estimated slip slope.

Change in vehicle mass affects the normal forces, as shown in Fig. 23. Fig. 24 shows that mass change also affects the estimates of the longitudinal forces. If mass increases, the longitudinal forces will increase or if mass decreases, the longitudinal forces will decrease.

Fig. 25 shows the effect of mass change on normalized traction forces. The normalized traction forces change only a little because when mass increases, longitudinal forces and normal forces both increase. Since normalized traction forces change only a little, the slip slopes also change only a little. Fig. 26 shows the effect of mass change on slip slopes. Thus, it can

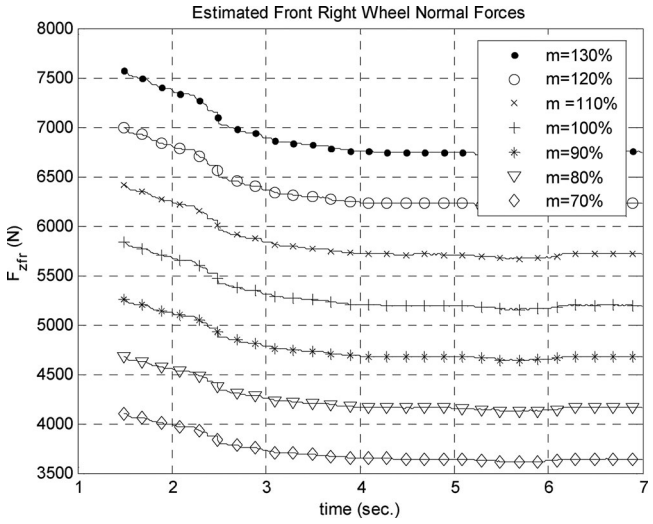

Fig. 23. Estimate front right wheel normal forces.

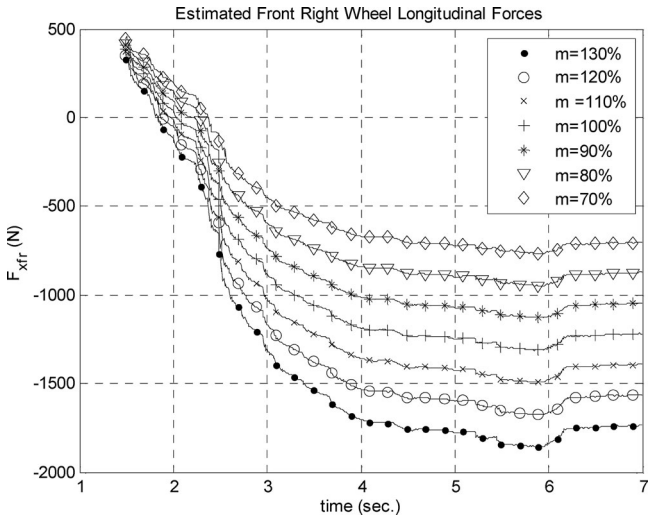

Fig. 24. Estimated front right wheel longitudinal forces.

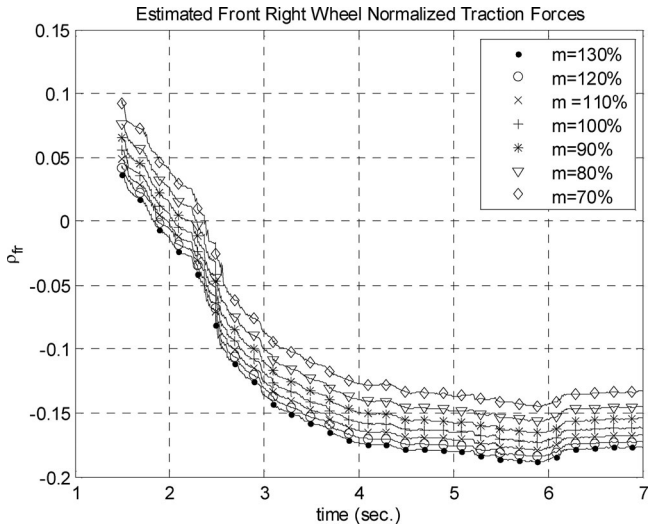

Fig. 25. Estimated front right wheel normalized traction forces.

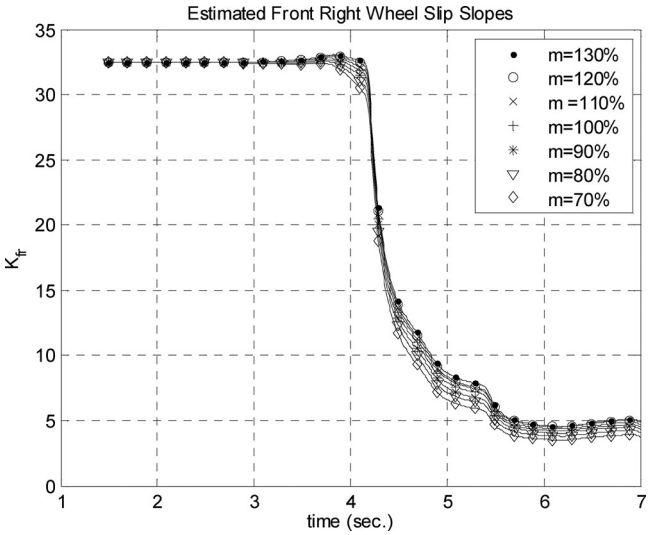

Fig. 26. Estimated front right wheel slip slopes.

be concluded that this friction estimation algorithm is robust to changes in vehicle mass.

X. Conclusion

This paper has focused on the development and evaluation of individual wheel friction coefficient estimation algorithms. Three different algorithms were proposed based on the types of sensors available—one that utilizes engine torque, brake torque, and GPS measurements; one that utilizes torque measurements and an accelerometer; and one that utilizes GPS measurements and an accelerometer. The developed algorithms were first evaluated in simulation using an industry-standard simulation software CARSIM and then evaluated experimentally on a Volvo XC90 sport utility vehicle. Experimental results demonstrate that friction coefficients at the individual wheels and road gradient can both be estimated quite reliably. While GPS measurements are subject to long-time dropouts in urban environments, brake torque and engine torque signals may not be available on all cars. Thus, each of the three algorithms has different application domains. When engine and brake torque measurement signals are available, the algorithm based on their use provides the best performance among the three algorithms.

Individual wheel friction measurements are expected to be more valuable for active safety systems than average friction measurements.

Acknowledgments

The experimental tests described in this paper were conducted at the Eaton Proving Ground in Marshall, MI.

References

[1] B. Breuer, U. Eichhorn, and J. Roth, "Measurement of tyre/road friction ahead of the car and inside the tyre," in *Proc. AVEC'92*, 1992, pp. 347–353.

[2] D. Bevly, J. C. Gerdes, and C. Wilson, "The use of GPS based velocity measurements for measuring side slip and wheel slip," *Vehicle Syst. Dyn.*, vol. 38, no. 2, pp. 127–147, Aug. 2002.

[3] U. Eichhorn and J. Roth, "Prediction and monitoring of tyre/road friction," in *Proc. FISITA*, 1992, pp. 67–74.
[4] F. Gustaffson, "Slip-based tire-road friction estimation," *Automatica*, vol. 33, no. 6, pp. 1087–1099, 1997.
[5] H. Dugoff, P.S. Fancher, and L. Segal, "Tyre performance characteristics affecting vehicle response to steering and braking control inputs," Office Vehicle Syst. Res., U.S. Nat. Bureau Standards, Final Rep. Contract CST-460, 1969.
[6] J. O. Hahn, R. Rajamani, and L. Alexander, "GPS-based real-time identification of tire-road friction coefficient," *IEEE Trans. Control Syst. Technol*., vol. 10, no. 3, pp. 331–343, May 2002.
[7] W. Hwang and B. S. Song, "Road condition monitoring system using tire-road friction estimation," in *Proc. AVEC*, Ann Arbor, MI, Aug. 2000, pp. 437–442.
[8] S. Müller, M. Uchanski, and J. K. Hedrick, "Estimation of the maximum tire-road friction coefficient," *ASME J. Dyn. Syst., Meas., Control*, vol. 125, pp. 607–617, Dec. 2003.
[9] R. Rajamani, *Vehicle Dynamics and Control*. New York: Springer-Verlag, 2005.
[10] L. R. Ray, "Nonlinear tire force estimation and road friction identification: simulation and experiments," *Automatica*, vol. 33, no. 10, pp. 1819–1833, 1997.
[11] H. E. Tseng, B. Ashrafi, D. Madau, T. A. Brown, and D. Recker, "The development of vehicle stability control at ford," *IEEE/ASME Trans. Mechatronics*, vol. 4, no. 3, pp. 223–234, Sep. 1999.
[12] A. T. Van Zanten, "Bosch ESP systems: Five years of experience," *SAE Trans*., vol. 109, no. 7, pp. 428–436, 2000.
[13] J. Wang, L. Alexander, and R. Rajamani, "Friction estimation on highway vehicles using longitudinal measurements," *ASME J. Dyn. Syst., Meas., Control*, vol. 126, no. 2, pp. 265–275, Jun. 2004.
[14] K. Yi, J. K. Hedrick, and S. C. Lee, "Estimation of tire-road friction using observer based identifiers," *Vehicle Syst. Dyn*., vol. 31, pp. 233–261, 1999.
[15] S. Sastry and M. Bodson, *Adaptive Control: Stability, Convergence and Robustness*. Englewood Cliffs, NJ: Prentice-Hall, 1989.
[16] D. Lhomme-Desages, C. Grand, J.-C. Guinot, and F. Ben Amar, "Doppler based ground speed sensor fusion and slip control for a wheeled rover," *IEEE/ASME Trans. Mechatronics*, vol. 14, no. 4, pp. 484–492, Aug. 2009.
[17] A. S. Conceicao, A. P. Moreira, and P. J. Costa, "Practical approach of modeling and parameter estimation for omnidirectional mobile robots," *IEEE/ASME Trans. Mechatronics*, vol. 14, no. 3, pp. 377–381, Jun. 2009.
[18] D. Zhao, X. Deng, and J. Yi, "Motion and internal force control for omnidirectional wheeled mobile robots," *IEEE/ASME Trans. Mechatron*., vol. 14, no. 3, pp. 382–387, Jun. 2009.
[19] L. R. Ray, "Experimental determination of tire forces and road friction," *Proc. Amer. Control Conf*., Jun. 1998, pp. 1843–1847.

Rajesh Rajamani received the B.Tech. degree from the Indian Institute of Technology, Madras, India, in 1989, and the M.S. and Ph.D. degrees from the University of California, Berkeley, in 1991 and 1993, respectively.

He is currently a Professor of Mechanical Engineering at the University of Minnesota, Minneapolis. He has authored over 80 journal papers and is a coinventor on seven patent applications. He is the author of *Vehicle Dynamics and Control* (Springer-Verlag, 2005). His research interests include sensors and control systems for automotive and biomedical applications.

Dr. Rajamani has served as the Chair of the IEEE Technical Committee on Automotive Control and on the editorial boards of the IEEE TRANSACTIONS ON CONTROL SYSTEMS TECHNOLOGY and the IEEE/ASME TRANSACTIONS ON MECHATRONICS. He is the recipient of a CAREER Award from the National Science Foundation, the 2001 Outstanding Paper Award from the IEEE TRANSACTIONS ON CONTROL SYSTEMS TECHNOLOGY, the Ralph Teetor Award from the SAE, and the 2007 O. Hugo Schuck Award from the American Automatic Control Council.

Gridsada Phanomchoeng received the B.S. degree in mechanical engineering from Chulalongkorn University, Bangkok, Thailand, in 2002, and the M.S. degree in aerospace engineering and mechanics from the University of Minnesota, Minneapolis, in 2007. He is currently working toward the Ph.D. degree in mechanical engineering at the University of Minnesota.

His research interests include advanced control system design, observer design for nonlinear systems, system identification, and applications to automotive systems.

Damrongrit (Neng) Piyabongkarn received the B.E. degree from Chulalongkorn University, Bangkok, Thailand, the M.S. degree from the University of Texas, Arlington, and the Ph.D. degree from the University of Minnesota, Minneapolis, all in mechanical engineering.

He is currently a Senior Control Systems Specialist Engineer at the Innovation Center, Eaton Corporation, Eden Prairie, MN. His research interests include advanced controls, system identification, and state estimation, with applications to automotive systems, hybrid systems, electro-hydraulic systems, and microsensor design.

Dr. Piyabongkarn was a recipient of the 2007 O. Hugo Schuck Award and a recipient of the SAE 2006 Arch Colwell Merit Award. He received the 2003–2004 Doctoral Dissertation Fellowship from the University of Minnesota.

Jae Lew received the Ph.D. degree in mechanical engineering from Georgia Institute of Technology, Atlanta, in 1993.

He has gained 18 years of research and teaching experience in the fields of control, dynamics, robotics, and mechatronics. This comprises some five years as a Research Scientist at Pacific Northwest National Laboratory, six years as an Assistant/Associate (tenured) Professor at Ohio University, and seven years as a Chief Engineer at the Eaton Innovation Center, Eden Prairie, MN. His research interests include applying modern control theory to electromechanical and hydraulic systems. Particularly, his work encompasses active damping and contact control of large structure systems including construction equipment and offshore applications; wind power drivetrain control; vehicle stability control systems with active differentials; and powertrain control of electrical/hydraulic hybrid vehicles. Currently, he is an Associate Editor for the IEEE TRANSACTIONS ON CONTROL SYSTEMS TECHNOLOGY.

Dr. Lew is a recipient of the ACC 2007 O. Hugo Schuck Award for the best application paper and the SAE 2006 Arch Colwell Merit Award.